AMERICAN METEOROLOGICAL SOCIETY
AMS Journals Online

AMS Home   Journals Home   Journal Archive   Subscribe   For Authors   Help   Advanced Search   [Search] Go

Full Text View

Eddies in the Labrador Sea as Observed by Profiling RAFOS Floats and Remote Sensing

Mark D. Prater

Graduate School of Oceanography, University of Rhode Island, Narragansett, Rhode Island

ABSTRACT

Data from profiling RAFOS floats, TOPEX/Poseidon altimetry, and the alongtrack scanning radiometer (ATSR) aboard *ERS-1* have been used to describe the spatial and seasonal patterns of eddy variability in the Labrador Sea. Peaks in sea surface height (SSH) variability appear in two regions: off the west Greenland shelf near 61.5°N, 52°W where the 3000-m isobath separates from the shelf, and in the center of the basin at 58°N, 52°W. Both locations show seasonal ranges in SSH variability of up to 40 mm, with the Greenland site, having largest variability in January–March, leading the central site by 50 days. A sea surface temperature image from the ATSR at the Greenland site shows numerous eddies, both cyclonic and anticyclonic, being formed by injection of West Greenland Current water into the Labrador Sea interior. Data from profiling RAFOS floats launched in 1997 as part of the Labrador Sea Deep Convection Experiment are used to describe three of the West Greenland Current eddies in detail. One of the sampled eddies was anticyclonic, while the other two were cyclonic. The eddies contained various mixtures of Irminger Sea Water. Peak azimuthal velocities ranged from 22 to 42 cm s^{-1}, and diameters from 20 to 50 km. Although the floats were at a depth of 375 m, the surface elevations derived from cyclogeostrophy agreed with those obtained from TOPEX/Poseidon. The temporal and spatial patterns in SSH variability are thought to be caused primarily by seasonal variations in the strength and stability of the West Greenland Current and, less likely, by eddy formation following deep convection in the basin interior.

Options:
- Create Reference
- Email this Article
- Add to MyArchive
- Search AMS Glossary

Search CrossRef for:
- Articles Citing This Article

Search Google Scholar for:
- Mark D. Prater

1. Introduction

The Labrador Sea is one of the few locations in the world's oceans that experiences deep convection, with complete mixing of the water column over the top 1500–2000 m. The mixed layer begins cooling in the fall, and by February the seasonal thermocline has been eroded away over large regions. The maximum mixed layer depths are typically observed in March. However, the restratification of the surface waters happens quickly; by May much of the upper water column (the top 200–500 m) has been restored to its preconvection state. To better understand the convection processes and water mass transformations in the Labrador Sea, an intensive observational program was sponsored by the Office of Navel Research's Accelerated Research Initiative of Oceanic Deep Convection (Lab Sea Group 1998). As part of this experiment, profiling RAFOS floats were deployed in the Labrador Sea from four cruises, spanning the time from fall 1996 to summer 1998. Unfortunately, a series of hardware and software problems diminished the anticipated amount of data to be recovered [details can be found in Prater et al. (1999)]. However, of the data recovered, the most striking features observed were of three eddies found near the west Greenland shelf. The appearance of these eddies with supporting data from satellite thermal images and altimetry indicated that eddies were common in the Labrador Sea. These eddies could act as the primary mechanism for homogenizing the intermediate waters of the Labrador Sea and for restratifying the upper waters. In addition, eddies can play a role in convection, by locally modifying the near-surface density structure and by trapping waters undergoing modification by atmospheric cooling (Legg et al. 1998).

Labrador eddies have been described before, but not always while in the Labrador Sea. Elliott and Sanford (1986) describe a lens of predominantly Labrador Sea origin, with core properties of 34.96 psu and 3.90°C. The vertical extent of the eddy was from 1000 to 3000 dbar, with the core at 1500 dbar. The eddy was anticyclonic, with a velocity maximum of 28.6 cm s^{-1} at a radius of 14.4 km. The eddy was found far from the Labrador Sea near 31°N, 70°W. Closer to the Labrador Sea, Pickart et al. (1996) found an extraordinarily weak eddy (maximum velocity of 0.5 cm s^{-1}) of upper Labrador Sea Water. This feature is perhaps better designated as a "blob" or pulse of distinct water property advected by the Labrador Current along the 2000-m isobath near Flemish Cap (49°N, 44°W). In the Labrador Sea, Gascard and Clarke (1983) used instruments similar to Swallow floats to observe an anticyclonic eddy with a radius of 10 km and maximum velocities of 24 cm s^{-1}. Hydrographic data supported the suggestion that the eddy was formed by the baroclinic instability of a rim current bordering a convectively mixed patch. Peterson (1987) used ice-floe motion in satellite imagery to observe nine cyclonic eddies along the 3000-m isobath in the northwest Labrador Sea. The radii of the eddies varied from 10 to 21 km, and maximum azimuthal velocities from 3 to 35 cm s^{-1}. Lilly and Rhines (2002) and J. M. Lilly (2001, personal communication) used moored current meter and hydrographic data from 56.75°N, 52.5°W to develop very detailed descriptions of Labrador Sea eddies. Lilly and Rhines presented six eddies that propagated through the mooring: four middepth, cold-core, anticyclonic eddies, and two upper-ocean, cyclonic warm-core eddies. The cold-core eddies had properties consistent with convectively mixed Labrador Sea Water, and are similar to the Elliott and Sanford (1986) feature. The shallower warm-core eddies had characteristics of Irminger Sea Water.

The purpose of this paper is to examine eddy variability in the Labrador Sea, initially motivated to understand the rapid restratification of the upper water column of the Labrador Sea after convection. The Labrador Sea, with TOPEX/Poseidon ground tracks, is shown in Fig. 1 ◉. A particularly striking sea surface thermal image of the Labrador Sea is presented and discussed in section 2, while sea surface height variability (as a surrogate for eddy activity) obtained from TOPEX/Poseidon altimetry is discussed in section 3. In section 4, three eddies observed by profiling RAFOS floats are described in detail. Finally, the paper is summarized and a few speculative hypotheses are given in section 5.

2. Alongtrack scanning radiometer

A unique view of the surface of the Labrador Sea was obtained from the alongtrack scanning radiometer (ATSR) on the European Space Agency's remote sensing satellite *ERS-1* (Mutlow et al. 1994). This satellite system views the sea surface in four infrared wavelengths, and as such can only derive SST for areas that are cloud-free [refer to Mutlow et al. (1994) for instrument description and processing algorithms]. An unusually clear view of the Labrador Sea occurred on 10 July 1992 and the resulting brightness temperature image for the 11-μm wavelength is shown in Fig. 2 ◉. The cold waters over the west Greenland shelf inshore of the 2000–3000 m isobath and in the northern reaches of the Labrador Sea are shown in purple, while the warmer waters of the central Labrador Sea are in red. The most striking features are the numerous swirls and eddies throughout the image. The eddies appear to be ejected from the west Greenland shelf at 61°N, 52°W, near the location where the 3000-m isobath separates from the coast. Numerous mushroom vortices (see Fedorov and Ginsburg 1986) consisting of paired cyclonic and anticyclonic eddies can be seen, along with individual eddies and other smaller scale temperature filaments, patches, and structures. One dipole eddy was observed that contained cold surface waters in its anticyclonic half, warmer waters in the cyclonic partner, and trailed a 50–100 km filament. The dipole is clearly seen as having been ejected from the frontal region in the center of the image. A subjectively derived inventory counted five dipole pairs and four other eddies with no discernible partner. The diameters of the eddies based on the sea surface temperature fronts ranged from 25 to 65 km. The polarities of the eddies were estimated by whether the small-scale temperature filaments associated with the eddies spiraled cyclonically or anticyclonically out from the center. The polarities appeared to be evenly distributed, with six cyclones, seven anticyclones, and one of undetermined rotation. The eddies were most prominent along and on either side of the 3000-m isobath after that contour separated from the shelf and turned to the southwest.

This same isobath has been observed in the analysis of both surface drifters (Cuny et al. 2002) and Profiling Autonomous Lagrangian Circulation Explorer (PALACE) floats at 700 m (Lavender et al. 2000) as a transition region between the strong cyclonic circulation crossing the Davis Strait along the 1000–2000 m isobath and the somewhat weaker anticyclonic flow in the basin interior. It is not known what role the eddies play in this transition. Are the eddies created and maintained by the counterrotating currents? Or is the anticyclonic current in the interior maintained by an eddy flux of vorticity? The very narrow temperature gradient along the west Greenland shelf shown in Fig. 2 ⊙▬ has broadened to 300 km in the center of the image. This could have been the result of eddies stirring the surface waters or simply the spreading of surface properties due to the barotropic components of the boundary current reacting to the divergence of the isobaths.

3. Sea surface variability from TOPEX/Poseidon altimetry

To quantify the sea surface variability (as a proxy for eddy activity) in the Labrador Sea, the Center for Meteorology and Physical Oceanography/Massachusetts Institute of Technology (CMPO/MIT) TOPEX/Poseidon Altimetric Data Set (King et al. 1994) was used. This dataset provided by CMPO/MIT has been pre-processed with all pertinent engineering, atmospheric, environmental, and tidal corrections incorporated. The data have been interpolated onto uniform 6.2-km alongtrack spacing. Only those data collected over "deep" water (greater than 1000 m) has been used so to minimize any effect of tidal model inaccuracies. Data from October 1992 to December 1998 was used in this analysis and consisted of 228 9.91-day repeat cycles. Since the primary interest was with the eddy activity in the Labrador Sea, there was no attempt to determine the absolute SSH by combining the altimeter data with an estimate of the earth's geoid or with dynamic height estimates from hydrography. Instead, the perturbation SSH was obtained with a two-step process. First, the SSH from each geographical point for all passes and for all cycles in the Labrador Sea was demeaned in an iterative manner whereby the time mean at each point was computed and then all data falling outside of two standard deviations from the mean were removed. This process was repeated three times to obtain a final demeaned SSH. Second, a linear fit was removed from the demeaned SSH of each pass through the Labrador Sea to act as a low-wavenumber filter.

The TOPEX/Poseidon footprint is nominally 2 km in calm sea conditions, but is a function of the sea state and increases to 10 km at the more extreme significant wave height of 10 m (Chelton et al. 1989). The sea state also affects the area of the ocean illuminated at any one time by the altimeter, described best as an annulus. The increasing sea state increases the radius of the annulus, but decreases the thickness of the band. Thus, the TOPEX/Poseidon altimeter measurement is not a "point" measurement, but is an average over a sea state (and hence somewhat seasonally) dependent area. The variation in area can cause the magnitude of the SSH estimate and hence the computed SSH variability to be biased downward. This is most noticeable as the eddy scale decreases; for example, measurements from a 10-km footprint can better reproduce the SSH structure of a 100-km diameter eddy than they can for a 10-km diameter eddy. If one knew both the sea state and the wavenumber spectrum of the eddy field, a correction could be made to estimates of altimeter-derived SSH variability and eddy kinetic energy. This was not done in this paper, but remains an area of further research.

The TOPEX/Poseidon data was segmented by season: January–March (JFM), April–June (AMJ), July–September (JAS), and October–December (OND). The standard deviation of the SSH values was computed at every grid point that had at least 25 good values in a season (approximately half of the total possible number of good data values). The resulting values were interpolated onto a uniform grid using a Gaussian smoother with a 50-km e-folding scale, and are shown in Fig. 3 ⊙▬ (the seasons progress clockwise from the upper left). The maximum variability occurred off the west coast of Greenland near 61°N, 52°W, in the identical location as the eddy activity observed by the ATSR and shown in Fig. 2 ⊙▬. The variability in this region (shown in yellows and reds) peaked in JMF near 80 mm and was reduced to 55 mm in JAS (the season of the ATSR image). This high variability region is centered on the location where the 3000-m isobath diverges from the shelf. It is presumed that the high levels of SSH variability were due to enhanced eddy formation from the West Greenland Current. No elevated SSH variability was visible elsewhere along the pathway of the West Greenland Current or the Labrador Current seaward of the 1000-m isobath. This indicates that those currents (other than in the vicinity of the SSH variability maximum) are very stable. The stability may be due, in part, to topographic effects (see Kearns and Paldor 2000).

A second maximum in SSH variability forms in the interior of the Labrador Sea at 58°N, 52°W, but is only evident during AMJ. This region's variability peaks at over 70 mm but is not a noticeable center of variability the rest of the year. The source of this variability is not immediately apparent. One hypothesis is that the eddies are an end product of deep convection. An idealized scenario is that localized cooling creates a spatially confined mixed layer. As cooling continues, a horizontal density gradient is formed between the mixed patch and the surrounding waters. A cyclonic rim current develops at this density gradient, and the current eventually generates meanders, via baroclinic instabilities, that grow and pinch off to form eddies (Visbeck et al. 1996; Jones and Marshall 1997; Marshall and Schott 1999). Although deep mixed layers can occur throughout the central Labrador Sea, the central region of the basin is not typically where the most intense convection occurs. Most evidence indicates that the deepest convection and the greatest heat flux occurs near the Labrador Shelf, where the continental winds are at their driest and coldest (Clarke and Gascard 1983; Lab Sea Group 1998; Pickart et al. 2002).

To examine the temporal structure of the SSH variability features in greater detail, two circular spatial domains were defined centered on the West Greenland and the Labrador Sea Basin variability maximums (see Fig. 1 ⊙▬). Each domain was approximately 300 km in diameter. Unlike the analysis presented above, where spatial maps of temporal variability were

presented, here a time series of spatial variability was considered. The assumption is that over a limited spatial domain the eddy field is homogeneous and is slowly varying in time. The data from within each 9.91-day cycle were processed as if it occurred simultaneously, and the standard deviation from all the TOPEX/Poseidon passes falling within each representative domain was computed. The results, spanning nearly six years, are shown in Figs. 4a and 4b ⬤￮. An annual variability cycle dominates, albeit with variability at both shorter and longer timescales. The annual ranges can often exceed 40 mm at each site. Large values occurred at the west Greenland site in early 1997 and 1998, while large values were found at the Labrador Sea Basin site in 1993, 1994, and 1997. A lagged correlation analysis showed that the peak near Greenland led the Labrador Sea peak by 50 days. The magnitudes of the annual maximums were compared to the winter (November–March) North Atlantic Oscillation (NAO) index [e.g., Hurrell (1995) and shown in Fig. 4c ⬤￮]. High values of the NAO index are indications of strong westerly winds, cold air, and increased Labrador Sea Water production. The higher SSH variability of 1993 and 1994 and the lower SSH variability in 1996 correspond to years of positive and negative NAO index. However, lower variability in the central Labrador Sea occurred during the highest NAO of this period (1995), while high variability occurred during a lower NAO (1997), although that year had a cold winter with convection in the Labrador Sea reaching to 1500 m (Pickart et al. 2002). Since both the NAO and SSH signals show considerable variability and are governed by dynamics acting on dramatically different temporal and spatial scales (decadal and basinwide for NAO, annual and mesoscale for SSH variability), a more detailed analysis will be needed to confirm their relationship.

Satellite altimetry has been used by several previous investigators to study the Labrador Sea. Han and Ikeda (1996) used complex empirical orthogonal function analysis to extract temporal and spatial patterns of SSH anomalies. They found a 50-mm annual signal in the mean, and attributed 80% of the variation to thermal expansion of the upper 500 dbar of the water column and only 20% to wind-driven effects. However, the wind effect on SSH was derived from a 1° by 1° barotropic numerical model, and thus the west Greenland and Labrador Currents were not resolved, nor were any baroclinic processes included. White and Heywood (1995) examined seasonal changes in the Labrador Sea as part of a larger study of the North Atlantic subpolar gyre. They found local maxima at the same two sites as described above, and noted that the eddy kinetic energy (EKE) in the Labrador Sea peaked in early March, while the wind stress curl peaks in mid-January. This timing is nearly identical to the time lag between variability maxima found in the west Greenland shelf and central Labrador Sea locations. White and Heywood postulate that large seasonal EKE signals can be attributed to eddy generation from wind stress, while seasonal cycles of smaller magnitude are found in regions dominated by baroclinic instability. White and Heywood also suggest that time lag between wind stress and eddy variability may be due to eddy energy being gained from the wind at a greater rate than it is lost after the wind stress peak has occurred.
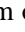
4. Eddy observations with profiling RAFOS floats

The profiling RAFOS float is based on the standard RAFOS float (Rossby et al. 1986), which is an acoustically tracked, neutrally buoyant, subsurface Lagrangian drifter. In the profiling version of the float, the electronics are contained within a glass pressure housing approximately 2.2 m in length and 0.095 m in diameter. The entire float weighs 17 kg in air. The float measures temperature and pressure at fixed time intervals and uses a hydrophone to record the times-of-arrival of acoustic signals transmitted from moored sound sources. The float is ballasted for a specified pressure surface and will remain on (or near) that surface collecting data until the preprogrammed mission terminates. At that time, the float releases a weight, rises to the surface, and transmits the data back to the user via the ARGOS satellite system. The float continues transmitting at the surface until its batteries are exhausted. The float's trajectory is computed in postprocessing using the locations of the sound sources, the float-recorded times-of-arrival, and values for the speed of sound appropriate for the study area.

The profiling version contains an internal volume changing (vocha) mechanism (Rossby et al. 1994) that consists of an internal motorized piston and seawater-filled cylinder connected to the outside of the float by a small tube. As the motor drives the piston forward into the cylinder, seawater is expelled, effectively decreasing the float's mass (or, equivalently, increasing its volume) and thus causing the float to become more buoyant. Likewise, when the motor draws the piston back out of the cylinder, seawater is drawn in, and the float gains mass (loses volume) and becomes less buoyant. These changes in buoyancy allow the float to move vertically through the water column, enabling it to make vertical temperature profiles. The vocha has 16 discrete positions, including full in or out, thus permitting the float to also become neutrally buoyant at intermediate depths. The floats deployed in the Labrador Sea and described here had equilibrium depths of 375 m and returned to these levels after profiling the top 800–1000 m of the water column. A typical preprogrammed mission had the float profile once every seven days. Between profiles (which take about six hours to complete), the float remained neutrally buoyant at a predetermined depth and made measurements of temperature (with a resolution of almost 0.001°C) and pressure (to 0.5 dbar) at 8-h intervals. An exception to this sampling schedule occurred between deployment and the first vertical profile at seven days, when these floats sampled at 2-h intervals.

To provide acoustic navigation for the RAFOS floats, four sound source moorings were deployed in the Labrador Sea from the C.S.S. *Hudson* in October–November 1996. The sound sources transmitted an 80-s tone six times a day (every 4 h), although our floats listened at 8-h intervals. We initially had concerns that, when the sound speed minimum rose to the surface during the winter convection period, the sound propagation distances would be so reduced as to make float tracking impossible. Fortunately, that was not the case, and high quality 400 km ranges were achieved even during the convection season.

The floats were deployed in the Labrador Sea with two separate purposes. First, floats were deployed in February and March of 1997 and 1998 in regions of deep convection. Those floats profiled to quantify the changes in the heat content of the water column in a Lagrangian framework and sampled temperature and pressure at 2–5 min intervals to estimate vertical velocities and (with less confidence) the vertical heat flux. The methodology and error estimates of these measurements can be found in Kearns and Rossby (1993) and Prater et al. (1999), with preliminary results given in Prater et al. (1999). The second purpose was to explore the rapid restratification (the reestablishment of the fresh and warm waters in the upper few 100 m) of the basin interior after convection. To that end, floats were deployed in the interior and near the west coast of Greenland. A series of hardware and software problems prevented many of the floats from returning data (Prater et al. 1999). However, three separate eddies were observed, and characteristics of each of these eddies will be described. Since each eddy was observed with one individual and separate float, the float numbers will be used to identify the eddy.

a. Float 404
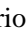
RAFOS float 404 had the longest eddy record of any of the profiling RAFOS floats, with 60 days in the eddy and making over 20 revolutions around the center (Fig. 5 ⬤). The float was deployed at 60.18°N, 48.68°W on 22 May 1997 from the C.S.S. *Hudson,* at a pressure level of 375 dbars in 2500 m of water. (All float deployments are given in Table 1 ⬤.) The float traveled northwestward following the coast for several days along the bathymetry until caught in a cyclonic eddy. The float remained in the eddy until the float's mission ended on 2 August 1997. The eddy's trajectory tended to follow the bathymetry in the Labrador Sea and always remained between the 2000- and 3000-m isobaths. The eddy underwent several stages of translational movement, nearly stationary at first, then moving at over 20 cm s^{-1} for 20 days, followed by a 50-day period of steady 10 cm s^{-1} movement [in the same range of velocities as found by Cuny et al. (2002) from surface drifters]. Finally, the eddy was again nearly stationary for the last 20 days of record.

To examine the eddy's structure, the mean motion of the eddy was removed from the position record. This was accomplished by a moving box-car filter of the float's positions, with a variable window length based on the orbital period of the float. Window lengths of 2.7–5.3 days (which correspond to 8–16 acoustic navigation fixes) resulted in the "best" (judged subjectively) trajectory of the eddy-referenced float (Fig. 6a ⬤). Azimuthal velocities (v_θ) were then computed using cubic splines of the trajectory and then differentiating the splined values at the times of the measured float locations. The radial distribution of v_θ is shown in Fig. 6b ⬤. The structure of the eddy is not readily apparent, but when the data are averaged in 2-km radial bins, the velocity is shown to increase radially to approximately 18 km. The error estimates for the binned mean velocity, shown by the solid vertical line extending plus/minus one standard deviation from the mean, are typically less than 4 cm s^{-1}. A subjective fit through the data is made, assuming a solid-body rotating core

$$v_\theta = V_{max}\left(\frac{r}{R_{max}}\right) \tag{1}$$

and a quadratic far field decay

$$v_\theta = V_{max}\left(\frac{R_{max}}{r}\right)^2, \tag{2}$$

where V_{max} is the maximum value of v_θ and R_{max} is the radius where V_{max} is observed. Although the radial gradient is discontinuous at $r = R_{max}$, this model is commonly used to describe eddy structure (e.g., Prater and Sanford 1994). Other formulations have been used to model velocity structure in eddies (r^{-1} decay, exponential decay, etc.); however, the differences in overall structure are minor. Values of $V_{max} = 40$ cm s^{-1} and $R_{max} = 18$ km were found to be consistent with the measured data. These values indicate an eddy with a vorticity Rossby number R_ζ, defined as $2\omega/f$ where ω is the angular velocity of the eddy and f is the Coriolis parameter, of 0.35 and a period of 3.3 days (Fig. 6b ⬤). The radial distance of the float from the center of the eddy varied from 10 to 20 km (Fig. 6c ⬤), while the azimuthal velocity ranged from 20 to 40 cm s^{-1} (Fig. 6d ⬤). The values of R_ζ ranged from 0.2 to nearly 0.5 (Fig. 6e ⬤). The characteristics of this and of the other eddies described in this paper are summarized in Table 2 ⬤.

The float made 10 profiles over the top 800 m of the water column. All the profiles were approximately one R_{max} from the eddy center, which is in the transition region between the homogeneous core and the surrounding ambient waters. Thus, the core properties of the eddy are not well measured by the float; however, for midlatitude eddies R_{max} is typically between

the radius of the core and the radius of the property front (Hebert et al. 1990; Prater and Sanford 1994). The profiles do show (Fig. 7 ○) a strong thermocline at about 50 m. The eddy was capped with cooler waters initially (below 3°C and not discernible in Fig. 7 ○) and transitioned to warmer waters later (above 5°C). To warm the upper 50 m by 2°C in 35 days requires a mean heat flux of over 135 W m^{-2}. The Comprehensive Ocean–Atmosphere Data Set (COADS; da Silva et al. 1994) mean climatology for June and July in the northwestern Labrador Sea shows an average heat flux of 120 W m^{-2} in the region of the eddy trajectory, suggesting that the surface layer temperatures above the float were consistent with local modification (in a Lagrangian sense) rather than exchange due to advection. The influence of local warming may effect the surface temperatures of the eddies shown in the ATSR image (Fig. 2 ○). However, from this record it is not obvious whether the eddy motion extended to the surface and the change in surface properties was purely due to local heat flux, or if the eddy was sliding under regions of varying T/S properties. The cold plume "descending" to nearly 200 m in profiles 3–5 (Fig. 7 ○) is more easily explained by the eddy (and float) advecting post by the upper ocean feature. The temperature at the level of the float remained near 3.8°C except during a brief period where the isotherms dipped, raising the float temperature to over 4°C. The decrease in temperature anomaly in the core of the eddies may not be entirely due to stirring as the eddies move away from the shelf, but also to an increase in the float's distance from the center of the eddy (Fig. 6 ○). The lifting of the isotherms at depth between profiles 3 and 4 is coincident with an increase in both v_θ and the radial distance of the float trajectory in the eddy, and also marked the float's movement away from the west Greenland shelf.

J. M. Lilly (2001, personal communication) investigated eddies that were advected past a mooring in the interior of the Labrador Sea, and found that very few of the eddies, only 2 out of 33, had cyclonic rotation. Those two eddies were thought to contain a mixture of Irminger Current water and Labrador Sea Water, with temperature and salinities at the depth of float 404 of approximately 3.0°–3.1°C and 34.83–34.84 psu. Cuny et al. (2002) presented a detailed upper ocean temperature cross-section of the Labrador Sea basin from the May 1997 C.S.S. *Hudson* cruise along the World Ocean Circulation Experiment (WOCE) AR7W hydrographic line. Their Fig. 9 ○ shows evidence of an eddy pair off the Greenland shelf, with a warmer (>4°C) anticyclone and a cooler (<3.5°C) cyclone at the depth of the float. However, their Fig. 9 ○ also shows that the anticyclonic (warm) feature is capped by cold west Greenland shelf water (<2.9°C) and the cyclonic (cool) feature is capped by somewhat warmer waters, in a manner similar to the surface temperatures of the vortex dipole shown in Fig. 2 ○. This is consistent with a dipole extension of D'Asaro's (1988) eddy generation mechanism. In this view, we assume that the inshore portion of the shelf current contains anticyclonic vorticity, with cold surface shelf waters over warm Irminger Sea Water. Likewise, the offshore portion of the current contains cyclonic vorticity, with warmer (not pure shelf) water over cooler (not pure Irminger) water. As the jet or squirt leaves the shelf, the dipole vortex forms with each eddy containing its source vorticity and water type. Thus, we might expect floats caught in cyclones to contain waters slightly cooler than the more pure Irminger Sea Water found along the west Greenland shelf.

b. Float 402

Float 402 was deployed on 31 May 1997 at 60.06°N, 52.47°W at a nominal depth of 375 dbars (Fig. 8 ○). For four weeks the float made large (50–100 km) meanders in the northeastern Labrador Sea at speeds of 30–70 cm s^{-1} until being caught in a cyclonic eddy. The eddy was nearly stationary at 60°N, 50°W for almost four weeks and had started to move northwest when the float mission ended on 29 July 1997. Removing the mean motion of the feature (in the same manner as described earlier for float 404) revealed an eddy approximately 10 km in diameter (Fig. 9a ○) with a radial structure consistent with a 10-km R_{max} and 22 cm s^{-1} V_{max} (Fig. 9b ○), which results in a mean core vorticity Rossby number of 0.35. The radial distance of the float from the eddy center varied from 10 to 15 km (Fig. 9c ○), while the azimuthal velocity ranged from 10 to 30 cm s^{-1} (Fig. 9d ○). The value of $R\zeta$ ranged from 0.1 to nearly 0.6 (Fig. 9e ○).

The float profiles (Fig. 10 ○) show an initial warming at 400 dbar, and a continual warming thereafter of the upper 150 dbar. The thermal stratification at the level of the float was highest at profile 2 ($\sim 4.2 \times 10^{-3}$°C m^{-1}), decreased by a factor of 2 by profile 4 (2.6×10^{-3}°C m^{-1}), then decreased by another factor of 2 by profile 5 (1.0×10^{-3}°C m^{-1}), marking the entrainment of the float into the eddy. A decrease of stratification would be expected, if the float was entrained into the core of an anticyclonic eddy, but the float should experience an increase of stratification entering the core of a cyclonic subthermocline eddy. Above the level of the float, near 200 dbar, the thermal stratification does increase from profile 2 to profile 5. This suggests that the eddy is centered at that shallower level, and that the level of the float was coincident with the reduced stratification below the cyclonic core. The float temperature indicated that the eddy contained mixed Irminger Sea Water.

c. Float 395

Float 395 was deployed on 1 June 1997 at 61.23°N, 50.38°W at a nominal depth of 375 dbar (Fig. 11 ○). Almost immediately the float made an anticyclonic loop near the shelf break, moved westward and made two more anticyclonic loops before surfacing on 20 June 1999. Since the float trajectory was relatively short, a simple uniform translation of the eddy was assumed, and a speed of $u = -8$ cm s^{-1} and $v = -2.5$ cm s^{-1} produced the best empirical eddy motion over the

final two loops (Fig. 12a ⊖). Using 5-km radial bins, an eddy structure consistent with a R_{max} of 25 km and a V_{max} of 42 cm s^{-1} was found (Fig. 12a ⊖), resulting in a mean core R_ζ of −0.27. Over the short time the eddy was monitored, the radial distance of the float from the eddy center varied from 15 to 30 km, its azimuthal velocity varied from 20 to 40 cm s^{-1}, and its core R_ζ varied from 0.15 to 0.30 (Figs. 12c–e ⊖).

During the interval between the first and second profiles (not shown), the float transitions from a regime where cooler waters (3.1°C) were overlying warmer waters at the float level (4.9°C) along the shelf break to a more homogeneous water upper layer (4.7°–4.8°C) slightly off the shelf. The temperature signature was likely from Irminger Sea Water, and both this eddy's warmer temperature and negative vorticity were consistent with the generation mechanism discussed earlier in this section.

d. Surface signature of Labrador Sea eddies

In order to directly compare SSH (η) perturbations as measured by TOPEX/Poseidon with the eddies tracked by floats, several assumptions were made. First, that there was little vertical shear between the level of the float and the sea surface— that is, that the flow was nearly barotropic and that the velocity structure as measured by the floats was maintained without modification to the surface. Second, that the SSH was in cyclogeostrophic balance with the velocity field. This relation states that

$$v_\theta f + \frac{v_\theta^2}{r} = g\frac{\partial \eta}{\partial r}. \tag{3}$$

The model velocity field for the eddy assumed here is the same as was used in the eddy descriptions above [Eqs. (1) and (2)]. Using those velocity relations in (3) and solving for η, one gets

$$\eta(r) = \frac{V_{max}}{2gR_{max}}\left(f + \frac{V_{max}}{R_{max}}\right)r^2 - \frac{3V_{max}R_{max}}{2g}\left(f + \frac{V_{max}}{2R_{max}}\right),$$
$$r < R_{max} \tag{4}$$

$$\eta(r) = -\frac{V_{max}R_{max}^2}{g}\left(\frac{f}{r} - \frac{V_{max}R_{max}^2}{4r^4}\right), \qquad r > R_{max}, \tag{5}$$

assuming the conditions that $\eta \rightarrow 0$ as $r \rightarrow \infty$ and the solutions are continuous at $r = R_{max}$. Only one TOPEX/Poseidon pass was found that intersected the core of a float-tracked eddy. The eddies are small ($R_{max} < 25$ km) compared with the separation distance between ground tracks (>100 km), and the TOPEX/Poseidon repetition cycle is 9.91 days, which allows an eddy 100 km across traveling at 10 cm s^{-1} to easily pass among the TOPEX/Poseidon ground tracks between cycles. A comparison of SSH from TOPEX/Poseidon and η estimated from (4) and (5) and the model eddy parameters obtained for float 404 is shown in Fig. 13 ⊖. The mean of the TOPEX/Poseidon data modeled η field was set equal to the mean of the modeled η field. The modeled SSH agrees with the TOPEX/Poseidon elevation anomaly with magnitudes over 150 mm, suggesting that the eddy did have a surface velocity signature and that the eddies tracked by the RAFOS floats are of the same type as observed by the ATSR and by TOPEX/Poseidon altimetry. The cross-sectional profile of SSH has a slightly steeper slope than the modeled η, which may be due to the simplistic eddy structure function chosen. The locations of the measured and modeled maximum SSH anomaly fall within 5 km of each other.

5. Discussion

Data from profiling RAFOS floats, TOPEX/Poseidon altimetry, and the alongtrack scanning radiometer (ATSR) aboard *ERS-1* have been used to describe the spatial and seasonal patterns of eddy variability in the Labrador Sea. All the measurement methods show eddy activity where the 3000-m isobath separates from the west Greenland shelf at 61.5°N, 52°W. Data from three profiling RAFOS floats were used to describe three distinct west Greenland shelf eddies in detail. One of the sampled eddies was anticyclonic, while the other two were cyclonic. Peak azimuthal velocities ranged from 22 to 42 cm s^{-1}, and radii from 10 to 25 km. One eddy was found to have a SSH signature of over 150 mm as measured by TOPEX/Poseidon altimetry and as inferred from combining subsurface (375-m depth) RAFOS float orbital velocities with a simple model of eddy structure. A very sharp east–west surface temperature gradient exists along the west Greenland shelf, where the transition between the cold shelf waters and and warmer Labrador Sea surface waters (a change of at least 4°C)

can occur within a few kilometers. That sea surface temperature gradient broadens significantly in the northern Labrador Sea, and that broadening might be caused by the stirring action of the upper-ocean eddies and the transport of cold shelf waters hundreds of kilometers into the interior of the Labrador Sea. The subsurface waters, at least down to 375 m and likely deeper, are being stirred as well. At that depth the warm (3.5°–5.5°C) and saline (34.9–35.0 psu) Irminger Sea Water is found as part of the West Greenland Current between the shelf break and the 3000-m isobath (Lazier 1973). The profiling RAFOS floats were in both mixed and more pure Irminger Sea Water regimes, and we speculate that at depth the eddies were actively transporting and stirring Irminger water into the Labrador Sea interior. This mechanism may participate in the rapid seasonal restratification of the Labrador Sea following convection.

The SSH variability has an annual cycle and peaks from January through March. If the levels of variability are entirely dependent on eddy formation from the West Greenland Current, then the stability of the current must also have a strong seasonal dependence. Greatbatch et al. (1990) noted that in March the wind stress anomaly is in the opposite direction of the West Greenland Current, while in July the stress is aligned in the direction of the current. The wind stress anomalies (although not the mean stress) are weak the rest of the year. The current also undergoes changes along its path; Krauss (1995) deployed surface drifters drogued to 100 m in the East Greenland Current. The drifters rounded Cape Farewell and continued northward in the West Greenland Current. The drifter velocities at 60.5°N were directionally steady with a maximum velocity of 73 cm s^{-1}. By 63°N the velocity had dropped to 42 cm s^{-1}, and the trajectories showed meandering and irregular motions.

A second maxima in SSH variability occurred in the center of the Labrador Sea at 58°N, 52°W and has an equally strong annual cycle. However, the central Labrador Sea variability peaks in April through June, and a time series analysis shows the peaks to occur approximately 50 days after the west Greenland shelf site. One possible hypothesis for the eddy variability in the central Labrador Sea is that the eddies are formed as a consequence of convection and therefore should appear during the later stages of the convection season, or after March. However, the most intense convection has been observed nearer the Labrador shelf (Gascard and Clarke 1983; Lab Sea Group 1998; Pickart et al. 2002), where the TOPEX/Poseidon data show the lowest SSH variability. A counterpoint is given by Lilly and Rhines (2002), who used current meter mooring data to observe four middepth intensified cold, fresh, anticyclonic eddies, with properties consistent with convectively modified Labrador Sea Water. The radius of the largest anticyclone was 15 km, while the other three were 5 km. The typical surface velocity signature was 10 cm s^{-1}. However, if these values are used with the cyclogeostrophic model presented earlier, the maximum sea surface displacement would only be 10 mm, which is well below the background SSH variability found in the Labrador Sea (Fig. 3 ⊙). Thus the variability mapped in this paper may not be a valid indicator of convective activity or intensity, at least in terms of middepth cold eddies. A more speculative hypothesis puts forth the idea that the export of Labrador Sea Water following convection would have a seasonal dependence, and hence there might be an increased demand for waters to replace the exported mass. Perhaps the surface variability maximum in the central Labrador Sea is the result of a seasonal transport of eddies from the west Greenland shelf site.

References

Chelton D. B., E. J. Walsh, and J. L. MacArthur, 1989: Pulse compression and sea level tracking in satellite altimetry. *J. Atmos. Oceanic Technol.*, **6**, 407–438. Find this article online

Clarke R. A., and J.-C. Gascard, 1983: The formation of Labrador Sea Water. Part I: Large-scale processes. *J. Phys. Oceanogr.*, **13**, 1764–1778. Find this article online

Cuny J., P. B. Rhines, P. P. Niiler, and S. Bacon, 2002: Labrador Sea boundary currents and the fate of the Irminger Sea Water. *J. Phys. Oceanogr.*, **32**, 627–647. Find this article online

D'Asaro E. A., 1988: Generation of submesoscale votices: A new mechanism. *J. Geophys. Res.*, **93**, 6685–6693. Find this article online

da Silva A. M., A. C. Young, and S. Levitus, 1994: Algorithms and Procedures. Vol. 1, *Atlas of Surface Marine Data 1994,* NOAA Atlas NESDIS 6, 84 pp.

Elliott B. A., and T. B. Sanford, 1986: The subthermocline lens D1. Part I: Description of water properties and velocity profiles. *J. Phys. Oceanogr.*, **16**, 532–548. Find this article online

Fedorov K. N., and A. I. Ginsburg, 1986: "Mushroom-like" currents (vortex dipoles) in the ocean and in a laboratory tank. *Ann. Geophys.*, **86**, 507–516. Find this article online

Gascard J.-C., and R. A. Clarke, 1983: The formation of Labrador Sea Water. Part I: Mesoscale and smaller-scale processes. *J. Phys. Oceanogr.*, **13**, 1779–1797. Find this article online

Greatbatch R. J., B. de Young, A. Goulding, and J. Craig, 1990: On the influence of local and North Atlantic wind forcing on the seasonal variation of sea level on the Newfoundland and Labrador Shelf. *J. Geophys. Res.*, **95**, 5279–5289. Find this article online

Han G., and M. Ikeda, 1996: Basin-scale variability in the Labrador Sea from TOPEX/POSEIDON and Geosat altimeter data. *J. Geophys. Res.*, **101**, 28325–28334. Find this article online

Hebert D., N. Oakey, and B. Ruddick, 1990: Evolution of a Mediterranean salt lens: Scalar properties. *J. Phys. Oceanogr.*, **20**, 1468–1483. Find this article online

Hurrell J. W., 1995: Decadal trends in the North Atlantic Oscillation: Regional temperatures and precipitation. *Science*, **269**, 676–679. Find this article online

Jones H., and J. Marshall, 1997: Restratification after deep convection. *J. Phys. Oceanogr.*, **27**, 2276–2287. Find this article online

Kearns E. J., and H. T. Rossby, 1993: A simple method for measuring deep convection. *J. Atmos. Oceanic Technol.*, **10**, 609–617. Find this article online

Kearns E. J., and N. Paldor, 2000: Why are the meanders of the North Atlantic Current stable and stationary? *Geophys. Res. Lett.*, **27**, 1029–1032. Find this article online

King C., D. Stammer, and C. Wunsch, 1994: The CMPO/MIT TOPEX/POSEIDON Altimetric Data Set. MIT Center for Global Change Science Rep. 30, 42 pp.

Krauss W., 1995: Currents and mixing in the Irminger Sea and in the Iceland Basin. *J. Geophys. Res.*, **100**, 10851–10871. Find this article online

Lab Sea Group, 1998: The Labrador Sea Deep Convection Experiment. *Bull. Amer. Meteor. Soc.*, **79**, 2033–2058. Find this article online

Lavender K. L., R. E. Davis, and W. B. Owens, 2000: Mid-depth recirculation observed in the interior Labrador and Irminger Seas by direct velocity measurements. *Nature*, **407**, 66–69. Find this article online

Lazier J. R. N., 1973: The renewal of Labrador Sea Water. *Deep-Sea Res.*, **20**, 341–353. Find this article online

Legg S., J. McWilliams, and J. Gao, 1998: Localization of deep ocean convection by a mesoscale eddy. *J. Phys. Oceanogr.*, **28**, 944–970. Find this article online

Lilly J. M., and P. B. Rhines, 2002: Coherent eddies in the Labrador Sea observed from a mooring. *J. Phys. Oceanogr.*, **32**, 585–598. Find this article online

Marshall J., and F. Schott, 1999: Open-ocean convection: Observations, theory, and models. *Rev. Geophys.*, **37**, 1–64. Find this article online

Mutlow C. T., A. M. Závody, I. J. Barton, and D. T. Llewellyn-Jones, 1994: Sea surface temperature measurements by the along-track scanning radiometer on the *ERS-1* satellite: Early results. *J. Geophys. Res.*, **99**, 22575–22588. Find this article online

Peterson I., 1987: A snapshot of the Labrador Current inferred from ice-floe movement in NOAA satellite imagery. *Atmos.–Ocean*, **25**, 402–415. Find this article online

Pickart R. S., W. M. Smethie Jr., J. R. N. Lazier, E. P. Jones, and W. J. Jenkins, 1996: Eddies of newly formed upper Labrador Sea Water. *J. Geophys. Res.*, **101**, 20711–20726. Find this article online

Pickart R. S., D. J. Torres, and R. A. Clarke, 2002: Hydrography of the Labrador Sea during active convection. *J. Phys. Oceanogr.*, **32**, 428–457. Find this article online

Prater M. D., and T. B. Sanford, 1994: A meddy off Cape St. Vincent. Part I: Description. *J. Phys. Oceanogr.*, **24**, 1572–1586. Find this article online

Prater M. D., J. Fontaine, and T. Rossby, 1999: Profiling RAFOS floats in the Labrador Sea: A data report. Tech. Rep. 99-2, Graduate School of Oceanography, University of Rhode Island, 37 pp.

Rossby T., D. Dorson, and J. Fontaine, 1986: The RAFOS System. *J. Atmos. Oceanic Technol.*, **4**, 672–679. Find this article online

Rossby T., J. Fontaine, and E. F. Carter Jr., 1994: The f/h float—Measuring stretching vorticity directly. *Deep-Sea Res.*, **41**, 975–992. Find this article online

Visbeck M., J. Marshall, and H. Jones, 1996: Dynamics of isolated convective regions in the ocean. *J. Phys. Oceanogr.*, **26**, 1721–1734. Find this article online

White M. A., and K. J. Heywood, 1995: Seasonal and interannual changes in the North Atlantic subpolar gyre from Geosat and TOPEX/POSEIDON altimetry. *J. Geophys. Res.*, **100**, 24931–24941. Find this article online

---

Tables

TABLE 1. Profiling RAFOS floats in Labrador Sea eddies

| Float	Launch date	Latitude (°N)	Longitude (°W)	Pressure (dbar)	Surface date	Latitude (°N)	Longitude (°W)
395	1 Jun 1997	61.23	50.38	375	20 Jun 1997	61.91	53.61
402	31 May 1997	60.06	52.47	375	29 Jul 1997	60.69	50.38
404	22 May 1997	60.18	48.68	375	2 Aug 1997	59.94	58.83

Click on thumbnail for full-sized image.

TABLE 2. Labrador Sea eddy characteristics

| Eddy (float)	Days in eddy	Velocity (cm s^{-1})	Radius (km)	Vorticity Rossby number	Temperature (°C)
395	9	−42	25	−0.27	4.75
402	28	22	10	0.35	3.59
404	65	40	18	0.35	3.86

Click on thumbnail for full-sized image.

Figures
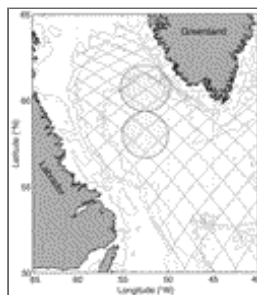
Click on thumbnail for full-sized image.

FIG. 1. The Labrador Sea Basin. The ground tracks of the TOPEX/Poseidon passes in the Labrador Sea are shown where the water depth exceeds 1000 m. The two shaded circles are the domains used in computing sea surface height variability from TOPEX/Poseidon data. Bathymetric contours are given at 200, 1000, 2000, 3000, and 4000 m.
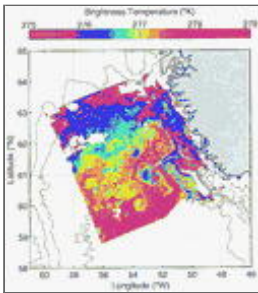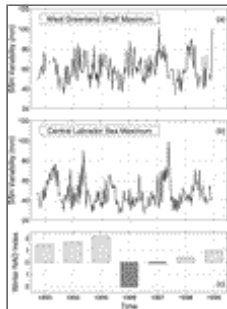
Click on thumbnail for full-sized image.

FIG. 2. Sea surface brightness temperature image of the the northern Labrador Sea from the ATSR on the *ERS-1* remote sensing satellite (from C. T. Mutlow 1999, personal communication). The image is from the 11-μm wavelength infrared sensor and shows numerous eddies near where the 3000-m isobath separates from the shelf
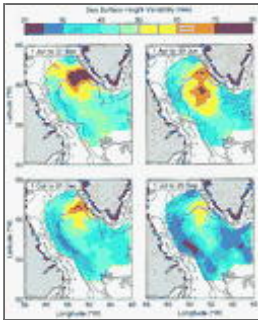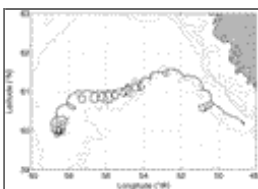

Click on thumbnail for full-sized image.

FIG. 3. Standard deviation of sea surface height anomaly as computed seasonally from six years of TOPEX/Poseidon altimetry data for the Labrador Sea. The seasons progress clockwise from the upper left

Click on thumbnail for full-sized image.

FIG. 4. Time series of spatial variability in sea surface height anomaly for the two regions showing local maxima: (a) the west Greenland shelf and (b) the central Labrador Sea. (c) The NAO index (from Joint Institute for the Study of the Atmosphere and Ocean at the University of Washington)

Click on thumbnail for full-sized image.

FIG. 5. Trajectory of float 404. Float profiles occurred at 7-day intervals and are labeled along the trajectory. Small dots denote each navigational fix and are given three times per day. The * marks the launch position
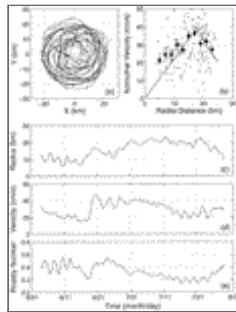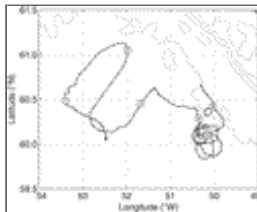
FIG. 6. Summary of the eddy characteristics of float 404. (a) Trajectory of the float relative to the translating center of the eddy. (b) Azimuthal velocity as a function of radial distance from the center of the eddy. Large black dots are average velocity in 2-km radial bins. Vertical black lines are ± the error of the mean. The thick gray line is a subjective model fit through the data. (c) Low-pass estimate of the float's radial distance from the center. (d) Low-pass estimate of the float's azimuthal velocity. (e) Low-pass estimate of the eddy's vorticity Rossby number
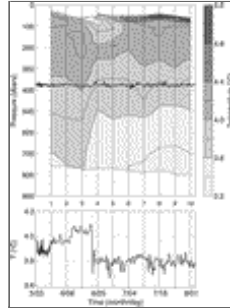
FIG. 7. Temperature and pressure records from float 404. (top) Contours of temperature from the float profiles. The solid line near 375 dbar is the pressure recorded by the float between profiles. (bottom) The temperature recorded by the float between profiles. The profile numbers are given between the two panels
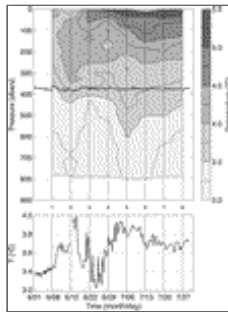
FIG. 8. Trajectory of float 402. Float profiles occurred at 7-day intervals, and are labeled along the trajectory. Small dots denote each navigational fix and are given three times per day. The * marks the launch position
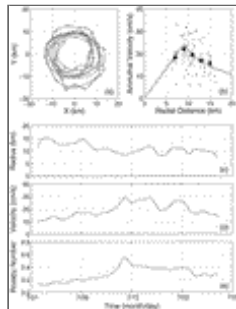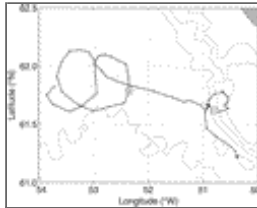
FIG. 9. Summary of the eddy characteristics of float 402. (a) Trajectory of the float relative to the translating center of the eddy. (b) Azimuthal velocity as a function of radial distance from the center of the eddy. Large black dots are average velocity in 2-km radial bins. Vertical black lines are ± the error of the mean. The thick gray line is a subjective model fit through the data. (c) Low-pass estimate of the float's radial distance from the center. (d) Low-pass estimate of the float's azimuthal velocity. (e) Low-pass estimate of the eddy's vorticity Rossby number
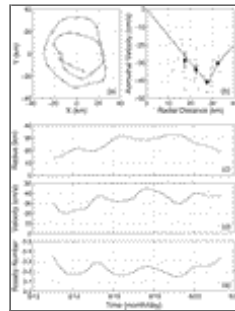
Click on thumbnail for full-sized image.

FIG. 10. Temperature and pressure records from float 402. (top) Contours of temperature from the float profiles. The solid line near 375 dbar is the pressure recorded by the float between profiles. (bottom) The temperature recorded by the float between profiles. The profile numbers are given between the two panels
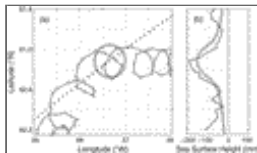

Click on thumbnail for full-sized image.

FIG. 11. Trajectory of float 395. Float profiles occurred at 7-day intervals, and are labeled along the trajectory. Small dots denote each navigational fix and are given three times per day. The * marks the launch position

Click on thumbnail for full-sized image.

FIG. 12. Summary of the eddy characteristics of float 395. (a) Trajectory of the float relative to the translating center of the eddy. (b) Azimuthal velocity as a function of radial distance from the center of the eddy. Large black dots are average velocity in 5-km radial bins. Vertical black lines are ± the error of the mean. The thick gray line is a subjective model fit through the data. (c) Low-pass estimate of the float's radial distance from the center. (d) Low-pass estimate of the float's azimuthal velocity. (e) Low-pass estimate of the eddy's vorticity Rossby number

Click on thumbnail for full-sized image.

FIG. 13. (a) TOPEX/Poseidon data locations (solid dots), Float 404 positions (open circles) and trajectory (solid lines), and location of eddy at the time of a TOPEX/Poseidon passover (large gray circle). (b) Comparison of TOPEX/Poseidon sea surface anomaly data (black line) and the modeled sea surface height from RAFOS float velocities (thick gray line)

Corresponding author address: Dr. Mark D. Prater, Graduate School of Oceanography, University of Rhode Island, South Ferry Rd., Narragansett, RI 02882. E-mail: mprater@gso.uri.edu